IEEE

PHOTONICS TECHNOLOGY LETTERS

A PUBLICATION OF THE IEEE PHOTONICS SOCIETY

This Print Collection Contains the Following Issues:

JANUARY 1, 2020	VOLUME 32	NUMBER 1	IPTLEL	(ISSN 1041-1135)
JANUARY 15, 2020	VOLUME 32	NUMBER 2		
FEBRUARY 1, 2020	VOLUME 32	NUMBER 3		
FEBRUARY 15, 2020	VOLUME 32	NUMBER 4		

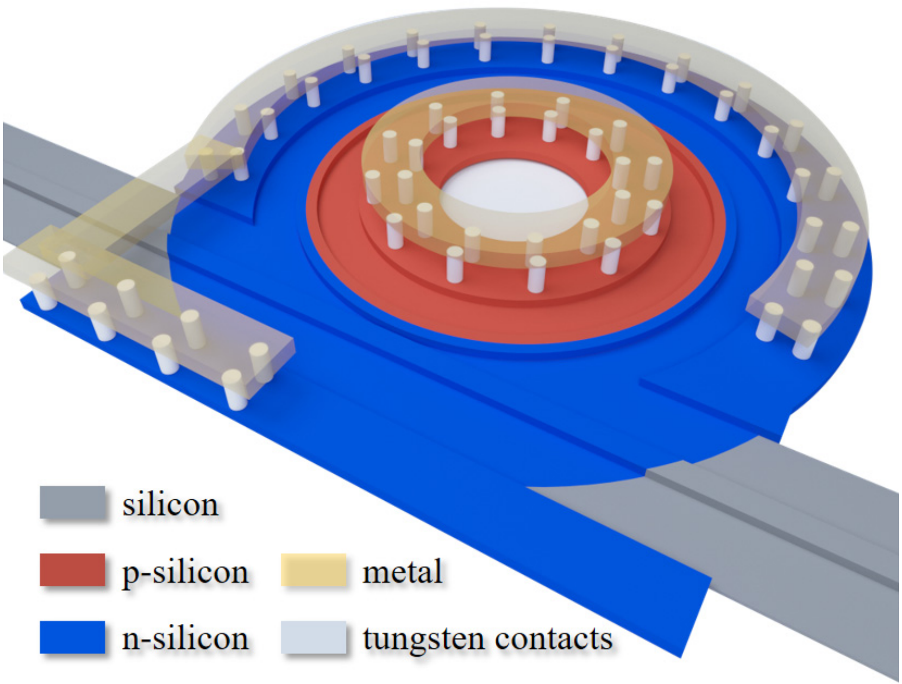

A single integrated silicon micro-ring modulator for a single-wavelength, single-polarization 160-Gbit/s four-level pulse amplitude modulation (PAM-4), as seen in "An Experimental Demonstration of 160-Gbit/s PAM-4 Using a Silicon Micro-Ring Modulator," by Y. Tong, *et al.*, p. 125.

For the January 1, 2020 issue, see p. 1 for Table of Contents
For the January 15, 2020 issue, see p. 75 for Table of Contents
For the February 1, 2020 issue, see p. 137 for Table of Contents
For the February 15, 2020 issue, see p. 179 for Table of Contents

Solution-Processed P3HT:PbS-Based NIR Photodetector With FET Configuration

Dan Yang and Qiang Zhou

***Abstract*— A solution-processed near-infrared (NIR) photodetector based on a mixture of PbS colloidal quantum dots (CQDs) and Poly(3-hexylthiophene) (P3HT) was presented. In a reverse field-effect transistor (FET) device configuration Au(S,D)/ P3HT:PbS/PMMA/Al(G), uniform-sized and well-dispersed PbS CQDs were employed as NIR absorbing materials in the active layer. Meanwhile, the poly(methyl methacrylate) (PMMA) dielectric layer could be seen as an encapsulation to enhance the device stability. Herein, high "on/off" current ratio (I_{on}/I_{off}) of 10^4 was obtained in dark, and the maximum photosensitivity (P) of 947 was gotten under 200 mW/cm^2 980 nm illumination. When the irradiance reduced to 0.1 mW/cm^2, the responsivity (R) and detectivity (D^*) of the NIR photodetector reached 9.4 mA/W and 2.5×10^{11} Jones, respectively. Therefore, the P3HT:PbS hybrid FET-based NIR photodetector had shown both relatively high electrical and detecting performance, which provided an experimental foundation and method for the next fabrication of medical infrared detectors and sensors.**

***Index Terms*— Near-infrared (NIR) photodetector, field-effect transistor (FET), PbS colloidal quantum dots (CQDs), Poly(3-hexylthiophene) (P3HT).**

I. Introduction

As an important member of optoelectronic devices, photodetectors have been extensively used in the national economy, military, healthcare, and other fields. Meanwhile, with rapid developments of optoelectronics and infrared technology, near-infrared (NIR) spectroscopy has gradually gained its wide applications on clinical medicine and pharmaceutical industry [1]–[3]. For these NIR spectrometers, photodetectors are the most important and essential elements, which performance affects the measure precision directly. Therefore, the high-performance and low-cost NIR photodetector has become a hot spot of research both in optoelectronic technique and medical instruments.

Field-effect transistors (FETs) are basic and important components in electronic circuits, which have been widely applied to integration, storage, amplification, rectification, and so on. Especially in detection, FET-based photodetectors exhibit greater optical gain, better responsivity, and higher signal-to-noise ratio than common photodetectors like photodiodes. The photodetector with FET configuration could separate photogenerated-carriers rapidly and extend the carrier recombination lifetime greatly through the modulation of gate bias, which overcomes shortcomings of excitons quenching and low optical gain. This kind of photodetector not only has the signal amplification function to realize excellent photoelectric detection, but also could be easily integrated in optoelectronic circuits.

Due to obvious material advantages of organic semiconductors (OSCs), large-area and flexible organic FETs have been intensively studied in recent years, which were often fabricated through easy-to-operate and low-cost solution processing methods [4]–[6], such as spin-coating, printing, and dip-coating. However, the absorption ranges of most OSCs are just in the visible region, which becomes a severe limitation on the incident light utilization and device applications. As hot materials of infrared optoelectronics, IV-VI Quantum Dots (QDs) based on the PbX (X = S, Se, Te) system [7]–[9] have exhibited excellent infrared properties because of the direct energy bandgap, large dielectric constants, potential for multiple-exciton generation, and a large Bohr radius. These special characteristics make their absorption peaks adjustable in a wide wavelength range from 800 nm to 3500 nm. That just covers the absorption shortage of OSCs in the infrared spectral region and improves performances of organic photoelectronic devices [10]–[13]. Therefore, we blended inorganic PbS CQDs and organic Poly(3-hexylthiophene) (P3HT) together to fabricate a kind of FET-based NIR photodetector through an easy solution method.

Recently, more and more studies focus on the solution-processed NIR photodetector. Zhao *et al*. fabricated an efficient Vis-NIR hybrid perovskite:PbS quantum dot photodetector using an antisolvent additive solution process, which exhibited a specific detectivity of 10^{11} Jones in the NIR region [14]. Lee *et al*. reported a high-detectivity flexible NIR photodetector prepared with redistributed Ag_2Se nanoparticles in aqueous inks for the first time. The device exhibited a high detectivity of 7.14×10^9 Jones at room temperature, delivering low power consumption, although it has undergone 0.38% compressive and tensile strains [15]. Zhu *et al*. prepared ultrasensitive PbSe quantum dots photodetectors with spectral response from 350 to 2500 nm by spin-casting, which exhibited over 120% EQE and D^* $\sim4\times10^{11}$ Jones in the infrared region [16]. In our experiments, PbS CQDs were chosen as the photosensitive material due to their strong infrared absorption

Manuscript received October 2, 2019; revised November 18, 2019; accepted November 27, 2019. Date of publication December 3, 2019; date of current version January 13, 2020. This work was supported in part by the Scientific Instrument Developing Project of the Chinese Academy of Sciences under Grant YJKYYQ20180068, in part by the Natural Science Foundations of Liaoning Province of China under Grant 2019-ZD-0333 and Grant 20180550122, and in part by the Scientific Project of Shenyang Medical College under Grant 20163044. *(Corresponding author: Dan Yang.)*

D. Yang is with the Department of Computer Science and Mathematics, Shenyang Medical College, Shenyang 110034, China (e-mail: yangdan1127@symc.edu.cn).

Q. Zhou is with the Institute of Applied Ecology, Chinese Academy of Sciences, Shenyang 110016, China (e-mail: zhouqiang@iae.ac.cn).

Color versions of one or more of the figures in this letter are available online at http://ieeexplore.ieee.org.

Digital Object Identifier 10.1109/LPT.2019.2957384

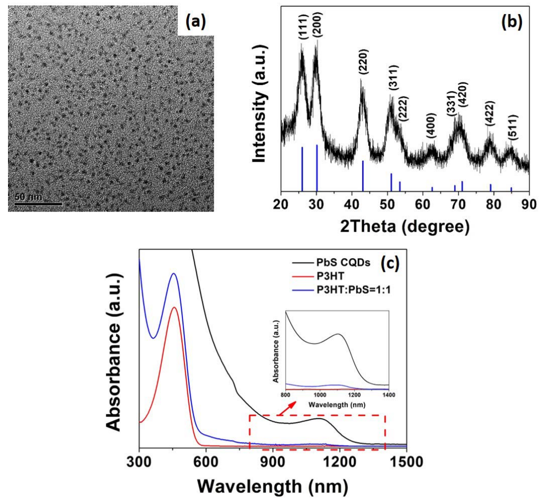

Fig. 1. TEM image (a), XRD pattern (b), and absorption spectra (c) of PbS CQDs.

and quantum confinement effect. P3HT was chosen as the carrier transport material due to its good solubility and film-forming property. These two kinds of semiconductors were mixed together to form the active layer by spin-coating. The top-gate/bottom-contact (TGBC) FET configuration was used as the basic structure of the NIR photodetector Au(S,D)/P3HT:PbS/PMMA/Al(G). High photosensitivity, responsivity and detectivity were obtained when the device was illuminated by a NIR laser, which provided an experimental foundation for the preparation of high-sensitivity, low-cost, large-area and flexible infrared photodetectors.

II. Experiments

PbS CQDs were synthesized based on a one-pot, hot injection method reported by Ma *et al.* [17], in which lead oxide (PbO, 99.9%) and bis(trimethylsilyl) sulfide (TMS,98%) were used as the lead and sulfur sources, respectively. The transmission electron microscopy (TEM) image and x-ray diffraction (XRD) pattern are shown in Fig. 1, as well as the absorption spectrum of PbS CQDs. With the average diameter of 3.5 nm, PbS CQDs exhibit uniform size distribution and good dispersibility in Fig. 1 (a). The XRD peeks in Fig. 1 (b) accurately correspond with the peaks from bulk PbS in the Joint Committee on Powder Diffraction Standards (JCPDS) reference diagram. From the absorption spectra in Fig. 1 (c), one can see feature peaks of PbS CQDs at 1100 nm and 750 nm, which are taken to correspond to the 1S-1S and 1S-1P transitions [18], [19], respectively. In contrast, pure P3HT has no absorption in the NIR region. By blending the two semiconductors together, PbS CQDs could extend the P3HT absorption range to the NIR region, which provides the key active material for the next NIR photodetector fabrication.

Fig. 2 shows the diagram of the TGBC FET-based NIR photodetector Au(S,D)/P3HT:PbS/PMMA/Al(G). Firstly, 50 nm gold drain and source electrodes were evaporated on a patterned ITO/glass substrate through an interdigitated shadow mask, which made the channel width to length ratio of 172. And then PbS CQDs and P3HT were sufficiently dissolved

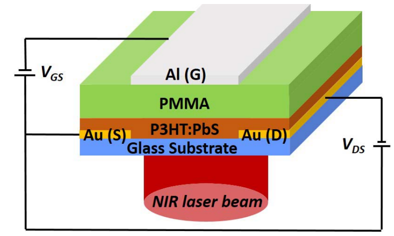

Fig. 2. Schematic illustration of the P3HT:PbS-based NIR photodetector with FET configuration.

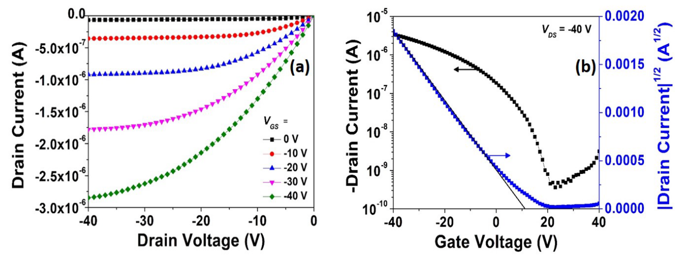

Fig. 3. Output characteristics (a) and transfer characteristics (b) of the NIR photodetector.

in chlorobenzene with the same weight ratio to form a 100 nm active layer by spin-coating. With the same simple method, a 80 mg/mL butyl acetate solution of poly(methyl methacrylate) (PMMA, MW = 120,000) was spin-coated on the P3HT:PbS film to form a 800 nm dielectric layer. Finally, an aluminum gate electrode with the thickness of 100 nm was prepared. The effective area of the photodetector is 4 mm^2, and all operations were done in the nitrogen-filled glove box. In the measurement, infrared laser with the wavelength of 980 nm was used as the incident light source to illuminate the device through the transparent glass directly.

III. Results and Discussion

A. Electrical Performance

The TGBC FET-based NIR photodetector has the same working principle with the organic field-effect transistor (OFET) in dark [17]. As shown in Fig. 2, the P3HT:PbS active layer is positioned between the Au source and drain electrodes. Current is injected from the source electrode into the active layer and collected by the drain electrode. The Al gate electrode is separated from the P3HT:PbS layer by the PMMA dielectric layer and controls the conductance of the active material in the channel region, with "on" or "off" states, by capacitively coupled by the PMMA layer. To investigate the basic electrical performance of the NIR photodetector, output and transfer characteristics were recorded by a Keithley semiconductor characterization system in dark, as shown in Fig. 3. The output characteristics in Fig. 3 (a) show the gate modulation of drain-source current (I_{DS}), one can clearly see the linear and saturation regions as the negative gate voltages increase, showing p-channel accumulation-type FET behaviors. Combining with the transfer characteristics in Fig. 3 (b), we could obtain the "on/off" current ratio (I_{on}/I_{off}) of 10^4 and the threshold voltage (V_{th}) of 11.3 V at a certain drain-source

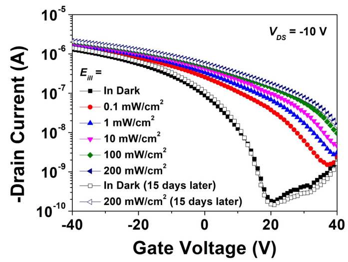

Fig. 4. Transfer characteristics of the NIR photodetector measured in dark, under illumination, and after 15 days of storage.

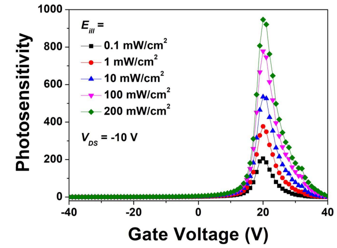

Fig. 5. P of the NIR photodetector as a function of V_{GS} under different illumination intensities.

voltage (V_{DS}). The V_{th} value is determined by the intercept of the ($|I_{DS}|^{1/2}$-V_{GS}) plot, and V_{GS} is the gate voltage. The carrier mobility (μ) is obtained from the saturation regime by the following Equation [20],

$$I_{DS} = 0.5WC_i\mu\left(V_{GS} - V_{th}\right)^2 \Big/ L \tag{1}$$

where C_i is the capacitance per unit area of the dielectric layer; W and L are the channel width and length, respectively. The capacitance is 2.6 nF/cm^2 measured through a parallel-plate capacitor structure, and the carrier mobility is 5.8×10^{-3} cm^2/V·s. This demonstrates the device has good electrical characteristics of p-type FET, which is beneficial to further NIR detection.

B. Detecting Performance

To investigate the detection performance of the NIR photodetector, transfer characteristics were measured under 980 nm illumination with different irradiance intensities, as shown in Fig. 4. One can see the curves have obvious positive shifts as the NIR light irradiance increases from 0.1 mW/cm^2 to 200 mW/cm^2. Keeping at the same V_{GS} as that in dark, I_{DS} at "off" state increases, which is due to the photovoltaic effect [21]. As soon as the 980 nm laser with photon energy higher than the bandgap energy of PbS CQDs (λ = 1100 nm) is absorbed, a number of photogenerated carriers are formed, and it leads to an increase in I_{DS} and an "on" state of the device. Meanwhile, the device generated more and more photo-induced carriers to increase I_{DS} with the incident irradiance intensities increasing. That amplified the current could directly reflect the information of the NIR light. Moreover, the same device was measured again after 15 days in dark and under illumination at 200 mW/cm^2. It could also be seen from Fig. 4, transfer characteristic curves measured 15 days later almost coincide with the fresh ones, implying that the device has good stability. That is mainly due to the uncommon TGBC FET configuration, in which the PMMA dielectric layer was prepared on the top of the P3HT:PbS active layer. The reverse fabrication seems like an encapsulation to prevent unstable PbS CQDs and P3HT from exposing in ambient air.

In addition to normal electrical parameters, photosensitivity (P), responsivity (R) and detectivity (D^*) are usually referred to as the key detecting parameters of FET-based photodetectors, which are expressed as following [22], [23],

$$P = I_{ph} \Big/ I_{dark} = \left(I_{illum} - I_{dark}\right) \Big/ I_{dark} \tag{2}$$

$$R = I_{ph} \Big/ P_{inc} = \left(I_{illium} - I_{dark}\right) \Big/ \left(E_{inc} \times A\right) \tag{3}$$

$$D^* = R \Big/ \left(2qJ_{dark}\right)^{1/2} \tag{4}$$

where I_{ph} is the photocurrent; I_{illum} and I_{dark} are the drain-source current under illumination and in dark, respectively. P_{inc} is the incident illumination power on the photodetector, which can be written as the product of the incident illumination irradiance E_{inc} and the effective area A of the photodetector. J_{dark} is the current density in dark and q is the electron charge.

Based on (2), P values of the NIR photodetector under illumination can be calculated in Fig. 5. Under the modulation effect of V_{GS}, the P maximum appears at "off" state of the device ($V_{GS} = -20$ V), not at "on" state. This is because field-induced charges dominate the conductivity at "on" state, and the effect of photogenerated carriers could not be seen obviously. When the device is charge-depleted at "off" state, photogenerated carriers contribute to I_{DS} mainly, which cause a noticeable change. The maximum P value is up to 947 when the irradiance increases to 200 mW/cm^2. At this special location, all detecting parameters are obtained by (2), (3), and (4). In Fig. 6(a), the maximum P and I_{ph} values increase with the irradiance enhancement, but the increase slows down in the later stage of larger irradiance, which is due to the accumulation of photogenerated electrons trapped by CQDs. From the energy level diagrams of P3HT/PbS in Fig. 6 (c), one can see that PbS CQDs absorb photons to generate electron-hole pairs under illumination. Because of the similar energy levels, photogenerated holes of the PbS CQDs could rapidly transfer to P3HT under V_{DS} to participate in conduction. However, the photogenerated electrons are trapped on the CQDs surfaces due to the large energy barrier. With increasing the irradiance intensity, more and more electrons accumulate on the surface of CQDs, which will cause a built-in electric field forming at the interface between PbS CQDs and P3HT. The electric field could hinder carriers from transporting at the CQD/P3HT interface, which is the reason of the saturated I_{ph} [24]. In Fig. 6 (b), R and D^* values reduce with increasing the irradiance intensity, and the maximum 9.4 mA/W and 2.5×10^{11} Jones appear at E_{ill} = 0.1 mW/cm^2. That demonstrates the device is more responsive to the weak NIR light, and also verifies the above explanation of I_{ph} saturation when the irradiance is too high. Therefore, such a kind of P3HT:PbS based NIR photodetector with FET configuration exhibits excellent electrical and detecting performance, which could provide a simple technique for the

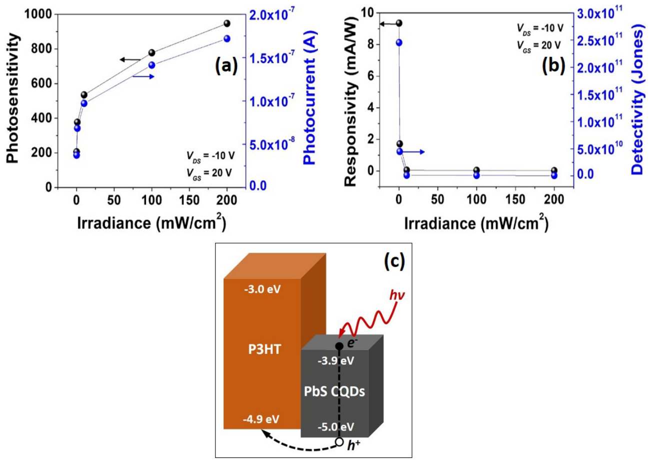

Fig. 6. P and I_{ph} curves (a) of the NIR photodetector measured under illumination together with R and D^* curves (b); (c) energy level diagrams of P3HT/PbS under illumination and charge carriers transport process.

further preparation of high-sensitivity and miniature medical infrared detectors and sensors.

IV. Conclusion

In conclusion, combining the optical property of PbS CQDs with the material property of P3HT, a kind of P3HT:PbS based NIR photodetector was successfully prepared by a simple spin-coating method. The TGBC FET configuration was employed as the basic device structure, in which the PMMA dielectric layer also acted an encapsulation. The device exhibited excellent electrical performance ($I_{on}/I_{off} = 10^4$, $V_{th} = 11.3$ V, $\mu = 5.8\times10^{-3}$ cm^2/V·s) and detecting performance (high P, R, and D^*) under 980 nm laser. When the irradiance was 200 mW/cm^2, the maximum P was up to 947, and the corresponding I_{ph} was 1.7×10^{-7} A. The device had better response to the weak light, the R and D^* reached the maximum value of 9.4 mA/W and 2.5×10^{11} Jones at $E_{ill} = 0.1$ mW/cm^2, respectively. With these good properties, this kind of NIR photodetector could supply an easy method for further preparation of high-sensitive and flexible infrared detectors, and provide a possibility for the miniaturization and low cost of medical infrared spectrometers.

References

[1] I. O. Afara *et al.*, "Characterizing human subchondral bone properties using near-infrared (NIR) spectroscopy," *Sci. Rep.*, vol. 8, no. 1, p. 9733, Jun. 2018.

[2] T. Monteyne *et al.*, "Analysis of protein glycation in human fingernail clippings with near-infrared (NIR) spectroscopy as an alternative technique for the diagnosis of diabetes mellitus," *Clin. Chem. Lab. Med.*, vol. 56, no. 9, pp. 1551–1558, May 2018.

[3] A. Sparén, M. Hartman, M. Fransson, J. Johansson, and O. Svensson, "Matrix effects in quantitative assessment of pharmaceutical tablets using transmission Raman and near-infrared (NIR) spectroscopy," *Appl. Spectrosc.*, vol. 69, no. 5, pp. 580–589, May 2015.

[4] F. Dai *et al.*, "Fabrication of two-dimensional crystalline organic films by tilted spin coating for high-performance organic field-effect transistors," *ACS Appl. Mater. Interfaces*, vol. 11, no. 7, pp. 7226–7234, Jan. 2019.

[5] S. M. Duan *et al.*, "Scalable fabrication of highly crystalline organic semiconductor thin film by channel-restricted screen printing toward the low-cost fabrication of high-performance transistor arrays," *Adv. Mater.*, vol. 31, no. 16, Apr. 2019, Art. no. 1807975.

[6] Z. Liu, H. Li, Z. Qiu, S.-L. Zhang, and Z.-B. Zhang, "SMALL-Hysteresis thin-film transistors achieved by facile dip-coating of nanotube/polymer composite," *Adv. Mater.*, vol. 24, no. 27, pp. 3633–3638, Jul. 2012.

[7] W. Ahmad *et al.*, "Lead selenide (PbSe) colloidal quantum dot solar cells with >10% efficiency," *Adv. Mater.*, vol. 31, no. 33, Aug. 2019, Art. no. 1900593.

[8] C. Ma, C. Shi, K. Lv, C. Ying, S. Fan, and Y. Yang, "Gradient-band-gap strategy for efficient solid-state PbS quantum-dot sensitized solar cells," *Nanoscale*, vol. 11, no. 17, pp. 8402–8407, Apr. 2019.

[9] D. M. Balazs *et al.*, "Stoichiometric control of the density of states in PbS colloidal quantum dot solids," *Sci. Adv.*, vol. 3, no. 9, Sep. 2017, Art. no. eaao1558.

[10] Y. Zhao, S. Yang, J. Zhao, and B. Zou, "PbS quantum dots based organic-inorganic hybrid infrared detecting and display devices," *Mater. Lett.*, vol. 196, pp. 176–178, Jun. 2017.

[11] M. Sulaman *et al.*, "High performance solution-processed infrared photodetector based on PbSe quantum dots doped with low carrier mobility polymer poly(N-vinylcarbazole)," *RSC Adv.*, vol. 6, no. 50, pp. 44514–44521, Apr. 2016.

[12] Z. X. Li *et al.*, "Enhancement of the power conversion efficiency of polymer solar cells by incorporating PbSe quantum dots," *J. Mater. Sci.*, vol. 50, no. 2, pp. 840–847, Jan. 2015.

[13] S. Y. Yang, N. Zhao, L. Zhang, H. Zhong, R. Liu, and B. Zou, "Field-effect transistor-based solution-processed colloidal quantum dot photodetector with broad bandwidth into near-infrared region," *Nanotechnology*, vol. 23, no. 25, May 2012, Art. no. 255203.

[14] D. Zhao, J. Huang, R. Qin, G. Yang, and J. Yu, "Efficient visible–near-infrared hybrid perovskite: Pbs quantum dot photodetectors fabricated using an antisolvent additive solution process," *Adv. Opt. Mater.*, vol. 6, no. 23, Dec. 2018, Art. no. 1800979.

[15] W.-Y. Lee *et al.*, "High-detectivity flexible near-infrared photodetector based on chalcogenide Ag_2Se nanoparticles," *Adv. Opt. Mater.*, vol. 7, no. 22, Nov. 2019, Art. no. 1900812.

[16] T. Zhu *et al.*, "Ultrasensitive solution-processed broadband PbSe photodetectors through photomultiplication effect," *ACS Appl. Mater. Interfaces*, vol. 11, no. 9, pp. 9205–9212, Feb. 2019.

[17] W. L. Ma, J. M. Luther, H. Zheng, Y. Wu, and A. P. Alivisatos, "Photovoltaic devices employing ternary PbS_xSe_{1-x} nanocrystals," *Nano Lett.*, vol. 9, no. 4, pp. 1699–1703, Feb. 2009.

[18] N. F. Borrelli and D. W. Smith, "Quantum confinement of PbS microcrystals in glass," *J. Non-Crystalline Solids*, vol. 180, no. 1, pp. 25–31, Dec. 1994.

[19] I. Kang and F. W. Wise, "Electronic structure and optical properties of PbS and PbSe quantum dots," *J. Opt. Soc. Amer. B, Opt. Phys.*, vol. 14, no. 7, pp. 1632–1646, Jul. 1997.

[20] Y. Guo, G. Yu, and Y. Liu, "Functional organic field-effect transistors," *Adv. Mater.*, vol. 22, no. 40, pp. 4427–4447, Oct. 2010.

[21] H.-S. Kang, C.-S. Choi, W.-Y. Choi, D.-H. Kim, and K. S. Seo, "Characterization of phototransistor internal gain in metamorphic high-electron-mobility transistors," *Appl. Phys. Lett.*, vol. 84, no. 19, pp. 3780–3782, Apr. 2004.

[22] M. C. Hamilton and J. Kanicki, "Organic polymer thin-film transistor photosensors," *IEEE J. Sel. Topics Quantum Electron.*, vol. 10, no. 4, pp. 840–848, Jul./Aug. 2004.

[23] X. Gong *et al.*, "High-detectivity polymer photodetectors with spectral response from 300 nm to 1450 nm," *Science*, vol. 325, no. 5948, pp. 1665–1667, Sep. 2009.

[24] S. M. Mok, F. Yan, and H. L. W. Chan, "Organic phototransistor based on poly(3-hexylthiophene)/TiO_2 nanoparticle composite," *Appl. Phys. Lett.*, vol. 93, no. 2, Jul. 2008, Art. no. 023310.